Journal of Power Sources 196 (2011) 2905–2912

Contents lists available at ScienceDirect

Journal of Power Sources

journal homepage: www.elsevier.com/locate/jpowsour

Thermomechanical analysis and durability of commercial micro-porous polymer Li-ion battery separators

Corey T. Love*

Alternative Energy Section, Code 6113, U.S. Naval Research Laboratory, 4555 Overlook Ave. S.W., Washington, DC 20375, USA

ARTICLE INFO

Article history:
Received 27 August 2010
Received in revised form 20 October 2010
Accepted 22 October 2010
Available online 3 November 2010

Keywords:
Polymer separator
Lithium ion battery
Thermomechanical analysis
Durability
DMA

ABSTRACT

Static and dynamic thermomechanical analysis was performed with a dynamic mechanical analyzer (DMA) to identify thermal and mechanical transitions for commercially available polymer separators under mechanical loading. Clear transitions in deformation mode were observed at elevated temperatures. These transitions identified the onset of separator "shutdown" which occurred at temperatures below the polymer melting point. Mechanical loading direction was critical to the overall integrity of the separator. Anisotropic separators (Celgard 2320, 2400 and 2500) were mechanically limited when pulled in tensile in the transverse direction. The anisotropy of these separators is a result of the dry technique used to manufacture the micro-porous membranes. Separators prepared using the wet technique (Entek Gold LP) behaved more uniformly, or biaxially, where all mechanical properties were nearly identical within the separator plane. The information provided by the DMA can also be useful for predicting the long-term durability of polymer separators in lithium-ion batteries exposed to electrolyte (solvent and salt), thermal fluctuations and electrochemical cycling. Small losses in mechanical integrity were observed for separators exposed to the various immersion environments over the 4-week immersion time.

Published by Elsevier B.V.

1. Introduction

Separator membranes are critical components of lithium-ion battery cells. Battery separators are micro-porous polymer membranes that electronically isolate the positive and negative electrodes, are easily wetted by an ion conducting liquid electrolyte and must be mechanically robust. While separators are electrochemically inactive components of a Li-ion cell, chemical degradation or mechanical failure of the separator in lithium ion battery cells can result in internal shorting and initiate thermal runaway [1,2]. The thermal stability of polymer separators is generally reported as the softening and melting temperatures. There is a need to characterize both the mechanical and thermal performance of polymer separators to understand how the membranes respond to elevated temperature under a constant or mechanical loading. Separators must be strong enough to withstand the cell winding process [3] and robust mechanical properties are necessary even above the shutdown temperature [4]. The purpose of this paper is to show the application of thermomechanical techniques to better characterize transition temperatures in polymer separators under static and dynamic loads as well as to observe mechanical durability due to environmental exposures: low temperature heating, electrolyte soaking, and electrochemical cycling.

The manufacturing process used to fabricate polymer separators dictates the orientation, size and shape of the pore structure as well as the crystallinity and mechanical behavior of the membrane. Two processing techniques are commonly used to produce micro-porous polymer separators for liquid nonaqueous lithium ion batteries. "Dry" processing of thermoplastic olefins utilizes extrusion to bring the polymer above its melting point and form it into the desired shape. Subsequent annealing and stretching processes may also be done to increase the crystallinity and orientation and dimension of the micropores [3,5]. Slit-like micropores or voids are formed by cold-drawing which causes stacked lamella to separate in the machine direction [6–8]. Upon cooling, crystallization of transverse tie-chains provide support for the porous structure. Orientation is dictated by annealing and extrusion at high speed and using high molecular weight polymers such as polyethylene and isotactic polypropylene [5,6]. The result is thicker and more pronounced lamella aligned along the extrusion direction after annealing [6] causing them to be anisotropic [9], meaning the mechanical properties along the extrusion direction (longitudinal) are superior to the lateral (transverse) direction [3]. "Wet" processing of polyolefin separators is done with the aid of a hydrocarbon liquid or low molecular weight oil mixed with the polymer resin in the melt phase [10]. The melt mixture is extruded through a die similar to the dry processed separators. Once in a sheet orienta-

* Corresponding author. Tel.: +1 202 404 6291; fax: +1 202 404 8119.
E-mail address: corey.love@nrl.navy.mil

0378-7753/$ – see front matter. Published by Elsevier B.V.
doi:10.1016/j.jpowsour.2010.10.083

Table 1
Technical data for commercially available polymer separators used in Li-ion battery cells.

Property	Commercial polymer separators[a]			
	Celgard® 2320	Celgard® 2400	Celgard® 2500	Entek® Gold LP
Material	PP/PE/PP	PP	PP	UHMWPE
Thickness, μm	20	25	25	19.4
Porosity, %	41	41	55	37
Pore size, μm	$d = 0.027$	$d = 0.043$	0.21×0.05	–
Gurley, s 100 cm^{-3} (JIS)	530	620	200	394
Puncture strength, g	360	450	>335	432

[a] Data taken from technical information brochures or certificate of analysis [12,21–23].

tion, the oil is extracted leaving behind a solid polymer membrane with random network of micro-voids. Since the structure of a wet-process separator is not induced mechanically, both pore structure and mechanical strength are not directionally dependent or oriented [10,11] and the separators are nearly isotropic within the film plane. A complete and comprehensive review of battery separators and manufacturing processes can be found in Refs. [3,10,11].

Four micro-porous polymer separators were obtained from two industry leading manufacturers. Table 1 provides the manufacturer specifications for the separators studied. Separators can exist as individual polymer films or multi-layered laminates. Celgard 2320 is a 3-layered laminate with a polyethylene (PE) core between two polypropylene (PP) skin layers. All other separators tested here are single-ply films. Celgard 2400 and 2500 are composed of single-layer isotactic polypropylene manufactured via thermal "dry" processing into axially oriented sheets. Scanning electron characterization by Sarada showed Celgard 2500 ellipsoidal pore dimensions to be 0.4 μm long and range from 0.2 to 0.15 μm wide [8] although these dimensions differ from the more recent technical data provided by the manufacturer [12]. Entek Teklon Gold LP separators are manufactured via the "wet" casting technique in which ultra-high molecular weight polyethylene (UHMWPE) is co-extruded with a plasticizer which is removed in post-processing [13] to yield a biaxially oriented cross-stitch pattern. The ASTM Gurley number is a membrane permeability indicator and is approximately proportional to the square of the tortuosity ($\sim\tau^2$) [14]. The lowest Gurley number is for 2500 which is expected due to its high porosity and large pore dimensions.

2. Experimental

X-ray diffraction (XRD) was done with a Bruker D8 Advance X-ray powder diffractomer to observe bulk crystallinity changes within the separators before and after environmental exposure. Crystallinity changes as a result of thermal rearrangement and molecular movement is best characterized with thermal analysis. Thermal properties such as melt temperature and melting endotherm were determined from simultaneous thermal analysis (STA). Polymer separator samples (10–15 mg) were loaded into uncovered alumina crucibles and heated from 35 °C to 700 °C at a heating rate of 10 °C min^{-1} under flowing argon. The degree of crystallinity was calculated according to Eq. (1) [15]:

$$X_c = \frac{\Delta H_m}{\Delta H_m^\circ} \times 100\% \quad (1)$$

where ΔH_m° is the melting enthalpy of a polymer single crystal with for polypropylene and $\Delta H_{m,PE}^\circ = 281.1\ J\ g^{-1}$ for polyethylene. The degree of crystallinity for the individual PE and PP crystalline components of the multi-layered Celgard 2320 should be considered an estimation with several assumptions. The estimation assumes uniform pore volume and thickness of the constituent layers and should not be considered a standard for the structural morphology of the separator.

Thermomechanical measurements were recorded with a TA Instruments 2980 DMA in tension to observe transitions in the bulk properties. Dimensional changes (shrink and elongation) were recorded under a static load of 0.015 N (1.8 g) for rectangular specimens (18 mm length × 9 mm width) while the temperature was increased 10 °C min^{-1} from 35 °C until the separator fractured or surpassed the travel distance of the DMA moving clamp (~40 mm). The percentage strain was calculated by Eq. (2) where $\%\varepsilon > 0$ implies a positive strain or film "extension" and $\%\varepsilon < 0$ implies a negative strain or film "shrinking." Three samples were tested under each condition.

$$\%\varepsilon = \frac{l - l_o}{l_o} \times 100\% \quad (2)$$

The application of a dynamic oscillatory force on the mechanical properties of polymer separators at elevated temperature was measured through DMA. A dynamic load of 0.015 N was applied at a frequency of 1 Hz to rectangular specimens (18 mm length × 9 mm width) in tension between 40 and 120 °C to analyze the material response (displacement, storage modulus, loss modulus and tan δ) to an oscillatory tensile force. The thickness of the specimens varied as shown in Table 1. The storage modulus, E', is the measure of the elastic energy stored within a material under deformation can be elucidated with this technique. The advantage of DMA is that we can obtain a modulus value each time a sinusoidal tensile force is applied across a temperature range [16]. This can be used to predict long-term performance at elevated temperatures and under applied mechanical loads. The above characterization technique was performed on "as-received" polymer separator materials as well as separators exposed to three separate conditioning environments: (1) 55 °C anneal in air for 4 weeks, (2) submersion in a 1 M $LiPF_6$ electrolyte in ethylene carbonate/propylene carbonate/dimethyl carbonate (1:1:2) solvents for 4 weeks, and (3) cycled in $LiCoO_2$/MCMB pouch cells between 3.0–4.1 V for 100 cycles.

3. Results and discussion

3.1. Physical characterization

3.1.1. Morphology

XRD patterns show a high degree of crystallinity and orientation, a result of the manufacturing process to fabricate these materials (Fig. 1). Celgard 2400 and 2500 have sharp and distinct peaks around $2\theta = 14.0°$, 17.0°, 18.5° which is characteristic of isotactic polypropylene [17]. The Entek Gold LP sample, Fig. 1(d), displays diffraction peaks at approximately 21.5° and 23.9° typical of semi-crystalline polyethylene with a high molecular weight [18]. The diffraction pattern for Celgard 2320, Fig. 1(a), displays both sets of peaks for polyethylene and polypropylene due to its multi-layered laminate design (PP/PE/PP). The XRD penetration depth is sufficient enough to resolve the under layer in a multi-layered separator. The effect of immersion environment: 55 °C anneal, and post electro-

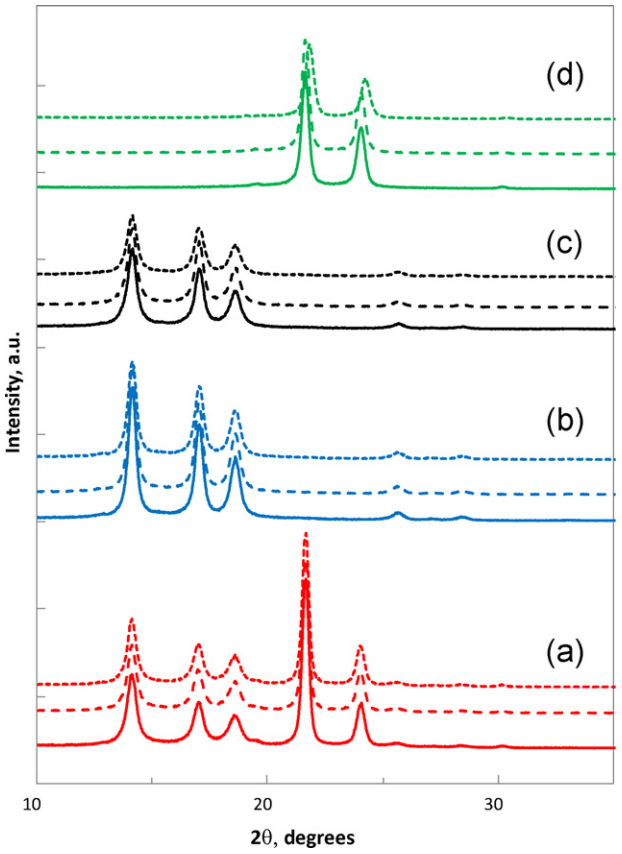

Fig. 1. XRD patterns of polymer separators (a) Celgard 2320; (b) Celgard 2400; (c) Celgard 2500; and (d) Entek Gold LP in the as-received (solid lines), after 55 °C anneal (dashed lines), and after cycling (dotted lines).

chemical cycling is also given in Fig. 1. There are no significant bulk structural changes between the as-received and conditioned materials. The Bragg diffraction angles and relative peak intensities match the initial conditions with the exception of cycled Entek Gold LP which displays a slight 2θ shift towards higher diffraction angles.

3.1.2. Thermal characteristics

The thermal decomposition data characteristic of the polymer separators is shown in Fig. 2. The decomposition temperature represents the onset of chemical degradation of the polymer species. The UHMWPE (Entek Gold LP) separator has a higher decomposition temperature than the PE and PP containing separators, around 420 °C. The tri-layer PP/PE/PP and Celgard 2500 (PP) separators have nearly identical decomposition profiles initiating around 390 °C. The lowest decomposition onset temperature is observed for Celgard 2400 (PP), 280 °C. No significant changes are observed in the thermal decomposition profiles of "as-received" and low temperature annealed separators. The thermogravimetric analysis of cycled separators (exposure of the polymer separator to both electrolyte and electrical current), Celgard 2320 and Celgard 2500, in Fig. 2(c) displays a different decomposition profile. The difference shown in the figure is due to the release of trapped solvent (Celgard 2320, 130–220 °C) and residual PVDF polymer binder from the pouch cell assembly (Celgard 2500, ~400 °C). The thermal decomposition of cell components: electrolyte solvent and salt, carbon, and PVDF were observed in most separators post cycling. This is a function of the pouch cell assembly and not the polymers propensity to adsorbed surface species. Mass loss has also been observed previously by Kostecki et al. for a similar polyolefin tri-layer separator immersed in a 1.2 M $LiPF_6$ in a mixture of ethylene carbonate/ethyl-methyl carbonate for 40 weeks at 55 °C [19]. In that work, an initial mass loss was observed due to trapped organic solvent within the porous membrane followed by the decomposition of phosphorous-containing products precipitated on the surfaces of the separator during storage at elevated temperature [19]. The degree of crystallinity calculated from the melting endotherms obtained from the DSC is listed in Table 2. The PP and PE layers of the Celgard 2320 separator are clearly distinguished with distinct melting endotherms at 135 °C ± 1 °C and 159 °C ± 1 °C, respectively. The single PP membranes maintained slightly higher melt temperatures of 161 ± 1 °C and 164 °C ± 1 °C.

Morphological changes resulting from the exposure environments can be observed through analysis of the melt behavior. Modest changes in the DSC melting endotherms of the polymer separators are observed after 4 weeks of annealing at 55 °C (Fig. 2(b)). The melt temperature for Entek Gold LP (UHMWPE) increases to 141 °C which may be due to increased thickness or perfection of lamellae [5]. Low temperature annealing causes a slight decrease in the melting endotherm peaks for PP separators (Celgard 2400 & 2500) with nearly identical melting temperatures. The multi-ply Celgard 2320 shows identical melt behavior for the PE component, but with decreased crystallinity and increased melting temperature for the outer PP skin layers. The lack of significant changes in the thermal characteristic indicates no chemical degradation after the 4-week immersion periods tested here.

3.2. Mechanical integrity-static loading

The effect of orientation of the mechanical load for Celgard 2320, a typical anisotropic multi-layered separator, is given in Fig. 3(a). When an external load is applied to an anisotropic separator in the axial direction with temperature, the porous structure of the membrane begins to collapse or "shrink" rapidly. This is the result of relieving internal stresses present in the membrane after stretching and quenching the membranes during fabrication. When the load is applied perpendicular to the axial-direction or the *transverse-direction*, the membrane undergoes 3-phases of deformation. Initially, the mechanical response is positive strain due to elastic creep. At or near the polymer melt temperature, the creep strain is recovered followed by shrinking (T_{shrink}). For the Celgard 2320 separator, the shrink temperature begins just before the melting temperature of the least thermally stable component, in this case PE at 130 °C. The highly oriented lamellar crystalline structure and the large number of stretched tie chains contributes to the high modulus of elasticity and reversible (recoverable) deformation [7]. The minimum negative strain associated with pore shrinking is termed here as the $T_{deformation}$. At $T_{deformation}$, strain induced necking begins and propagates along the drawing direction until

Table 2
Melt characteristics of polymer separators.

Property	Commercial polymer separators			
	Celgard® 2320	Celgard® 2400	Celgard® 2500	Entek® Gold LP
Melting temperature, °C	135.3, 159.0	161.7	164.6	137.1
Melting endotherm, J g^{-1}	32.4, 23.6	64.1	73.5	81.7
Degree of crystallinity, %	17, 33	31	35	29

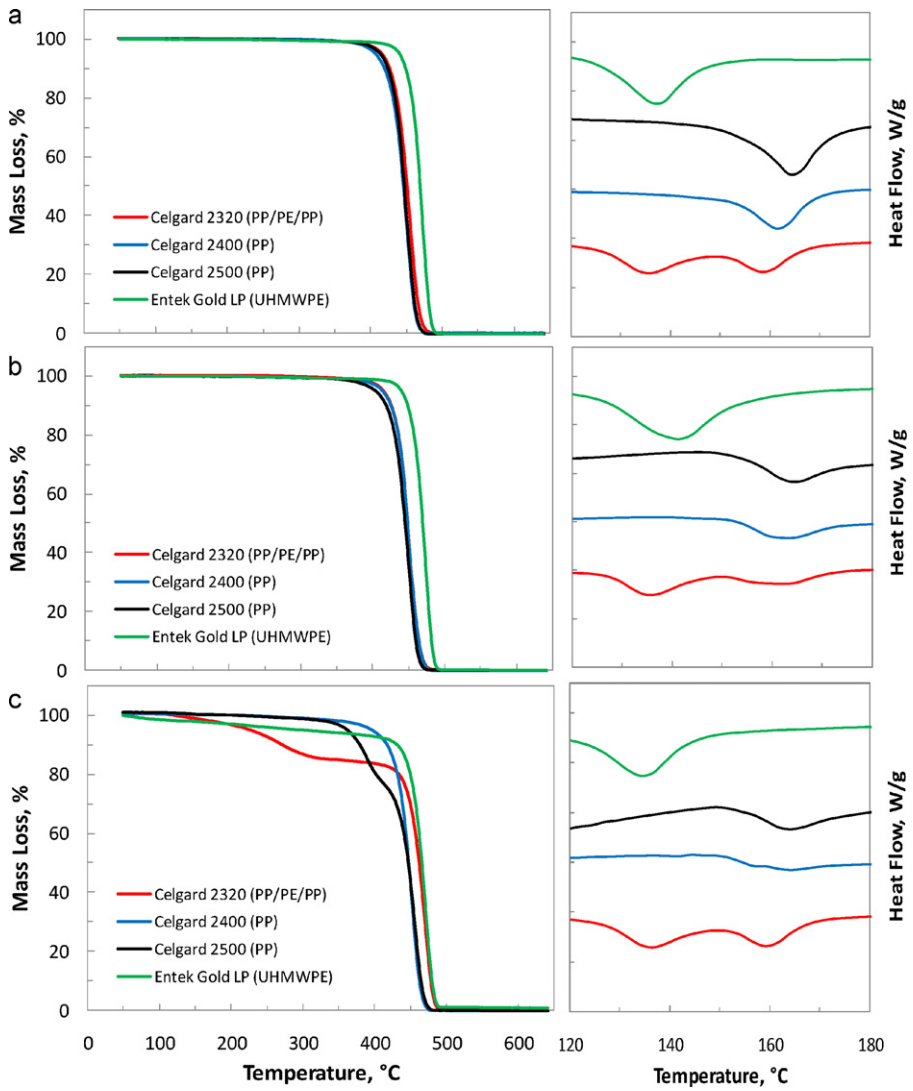

Fig. 2. Thermogravimetric analysis of as received polymer separators heated at 10 °C min^{-1} under argon and the corresponding DSC thermograms of polymer separators: (a) as-received; (b) after 55 °C anneal; and (c) after cycling.

the membrane ruptures at $T_{rupture}$. The temperature at zero strain is termed here T_0, the equilibrium temperature. T_0 identifies the region where elastic strain has been recovered to the zero strain position as a result of the onset of the pore shrink mechanism.

Anisotropic separators held under constant load in the axial-direction undergo a 2-phase failure mechanism, T_{shrink} and $T_{rupture}$, where the onset of shrink occurs well before the melt temperature (Fig. 3(a)). Shrinking continues until the separator has gone

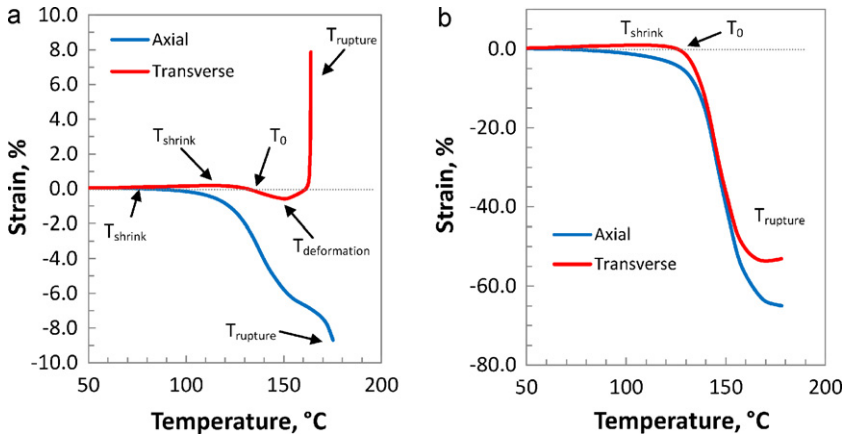

Fig. 3. Thermomechanical behavior of (a) Celgard 2320, an anisotropic battery separators (this behavior is also typical for polymer separators: Celgard 2400 and Celgard 2500) and (b) Entek Gold LP, a nearly isotropic biaxial battery separator, with static load applied in the axial and transverse-directions.

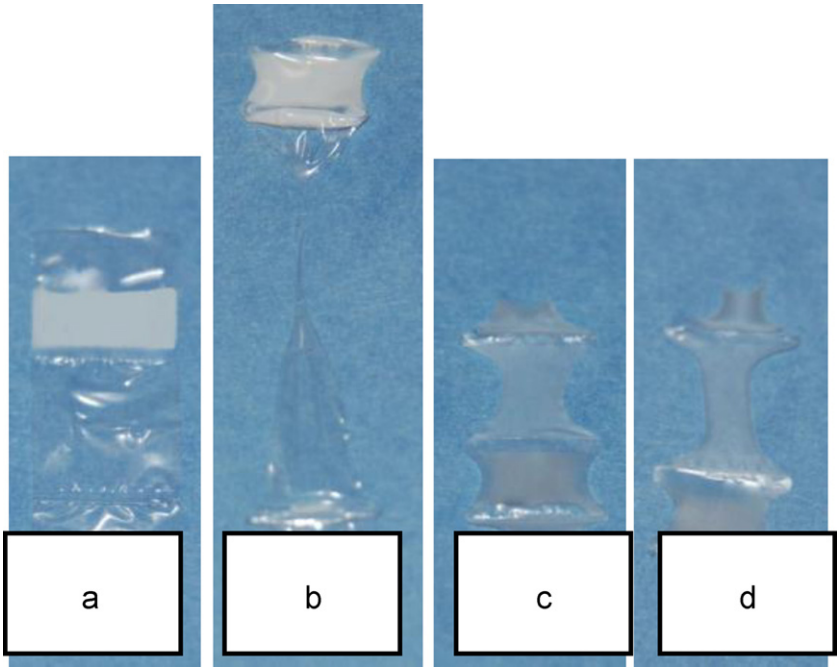

Fig. 4. The effect of temperature and loading direction on the physical deformation of polymer separators: (a) Celgard 2320 axial-direction; (b) Celgard 2320 transverse-direction; (c) Entek Gold LP axial-direction; and (d) Entek Gold LP transverse-direction.

into complete contraction but well before the thermal decomposition of the polymer. The two shoulders in the strain curve in the axial-direction of Fig. 3(a) are due to the multi-layered construction of PE and PP. Distinct features in the strain curve in the transverse-direction are not observed here to be materials dependent, but rather single shrink, deformation and rupture temperatures. The release of internal stress and shrink force is greater than the applied force which results in the overall negative strain. In the transverse-direction, the strain experienced by the weaker tie-chains dominates the initial failure mechanism. At the shrink temperature, the thermal energy causing a negative stain in the stronger perpendicular direction and as a result of Poisson's effects causes an overall shrinking. In the "as-received" state the polymer separators appear opaque. However, after thermomechanical testing of the polymers transition to completely transparent (Fig. 4). This transition is typically indicative of a crystalline to amorphous transition. In the case of the polymer separators, the increase in optical transparency is most likely due to inhomogeneities within the structure [20] as a result of mechanical and thermal stresses applied to the polymer. In the initial condition the separators are highly crystalline, however during deformation intermediate arrangements of spherulites become disordered leading to chain fracture and branching [20]. These flaws allow for transparency of the thermomechanical tested separators. To test this explanation, separators were placed in an oven set to the $T_{deformation}$ observed for the specific separator. After annealing at elevated temperature for several hours, the separators appear transparent as in shown in Fig. 4. The crystallinity of the annealed separators is confirmed with XRD where peak intensities were slightly diminished from the as-received state, but the existence of clear sharp peaks indicate the optical transparency of thermomechanically tested separators is due to structural flaws rather than a loss of crystallinity. The increase in clarity is most likely the result of a tensile stretching mechanism [20].

The biaxially-oriented separator, Entek Gold LP, exhibits nearly the same mechanical response when loaded in the axial and transverse-directions. Fig. 3(b) shows the strain curves as a function of temperature for the two loading configurations. It is evident the separators are not completely isotropic in-plane, since there are slight differences in the tensile response. Like the anisotropic Celgard, the biaxial Entek separator exhibits a 3-phase failure mechanism in the transverse-direction and only 2-phase failure in the axial-direction; however, the ultimate $T_{rupture}$ is nearly the same in both orientations and the transitions are not as dramatic as for anisotropic separators. This indicates there is a slight preferential strength to separators prepared using the wet technique, although the differences in mechanical response between the two loading orientations are minimal. The shrink temperature occurs at lower temperature for the axial-direction than the transverse orientation. For biaxial orientated separators such as Entek Gold LP there is not a dominant directionality and both axial and transversely loaded materials appear nearly identical after testing (Fig. 4).

According to Fig. 3, polymer separators are limited by thermo-mechanical properties in the transverse-direction. All thermo-mechanical data presented from here will therefore be with mechanical loading in the transverse direction; which is the limiting direction for mechanical properties of polymer separators. Fig. 5 illustrates the tensile response of the as-received polymer separators under constant load in the transverse-direction. The significant negative strain of the Entek Gold LP is due to the release of internal stresses in both directions of its cross-hatch morphology. The shrink, equilibrium, deformation and rupture temperatures for all separators are given in Table 3. For Celgard 2400 and Celgard 2500, separators of polypropylene material and the same thickness, are distinguished by percent porosity and pore dimension. The higher porosity of Celgard 2500 may initiate shrinking at lower temperature. It is difficult to correlate the effect of orientation for Entek Gold LP since the transverse biaxial contains longitudinally aligned segments. The direct correlation of mechanical data is complex due to the different materials, processing techniques, porosity, and pore dimensions. Celgard 2320 behaves as a single-ply with a single shrink, equilibrium, deformation and rupture temperature. The width and depth of the negative strain profile for 2320 shows the combined influence of PE and PP components; even though there is only a single deformation point.

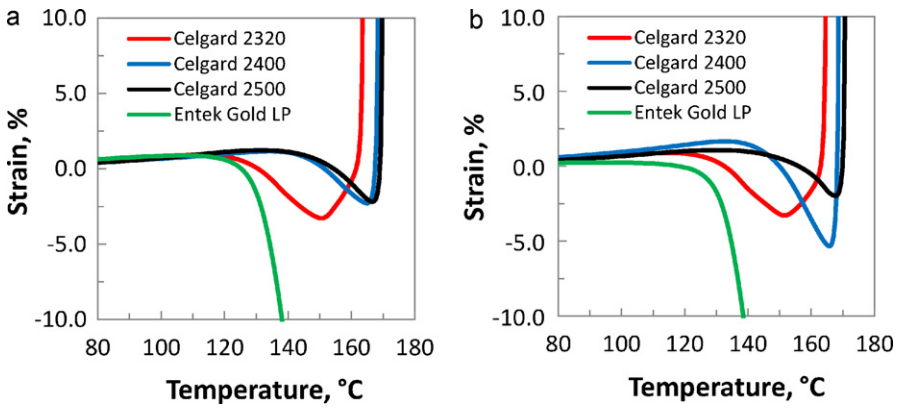

Fig. 5. Thermomechanical analysis of polymer separators under static tensile loading in the transverse orientation: (a) as-received and (b) after electrolyte soak.

3.2.1. *Effect of environments on mechanical integrity-static loading*

The effect of the exposure environments on the polymer separators mechanical integrity or durability is given in Table 3. Annealing at high temperature can increase the overall orientation of micro-porous polymers where orientation is attributed to lamellar orientation and molecular orientation [6]. No degradation in thermal or mechanical performance was observed for separators exposed to electrolyte during the short immersion period of this study. Slight changes in the thermal integrity after electrolyte exposure are within the ±1 °C sensitivity of the DMA instrument. The shrink, equilibrium, deformation and rupture temperature are nearly identical after immersion in electrolyte for 4 weeks. The shrink and equilibrium temperature for Entek Gold LP with electrolyte soak in the elastic region are lower although the deformation and rupture temperatures in the plastic deformation region match the as-received condition. It is speculated this is likely due to trapped electrolyte solvent and salt which could cause two weakening mechanisms. One mechanism suggests the reactivity of trapped solvent and lithium salt could initiate thermal decomposition just above 50 °C as seen in the thermogravimetric analysis (Fig. 2(c)). An alternative mechanism could be that the absorbed electrolyte solvent causes swelling or an artificial initial elastic strain on the Entek Gold LP separator. As the separator is heated, solvent is released causing the onset of elastic shrinking and the return to the zero-strain condition (equilibrium) to occur at lower temperatures. Once the solvent is completely removed the plastic deformation behavior should mimic that of the as-received condition.

3.3. *Mechanical integrity-dynamic loading*

The E' vs. temperature curves for polymer separators clearly identifies two modulus phases separated by a distinct transition temperature (Fig. 6). This transition takes place at the rubbery-to-viscous transition temperature, T_{trans}, which exists at one of the many transitions, observed for storage modulus versus temperatures for polymer materials. The transition temperatures reported in Table 4 are taken from the intersection of linear tangents. The severity of the slope (dE'/dT) indicates the degree of instability of the polymer at elevated temperature due to mechanically induced structure changes within the polymer and pore structure. Celgard 2320 displays a gradual softening of the membrane until T_{trans} = 110 °C. Fig. 7 shows the dimensional and transparency changes that resulted from the thermal and mechanical stresses placed upon the separator during dynamic thermomechanical characterization. In the weaker, transverse orientation, there is a greater degree of shrinking or negative strain. Additionally, necking is observed indicating a positive strain in the loading direction. Generally, separators loaded in the axial orientation retain their shape with slight shrinking in both *x*- and *y*-directions. After DMA testing, Celgard 2320 underwent a change from opaque to transparent,

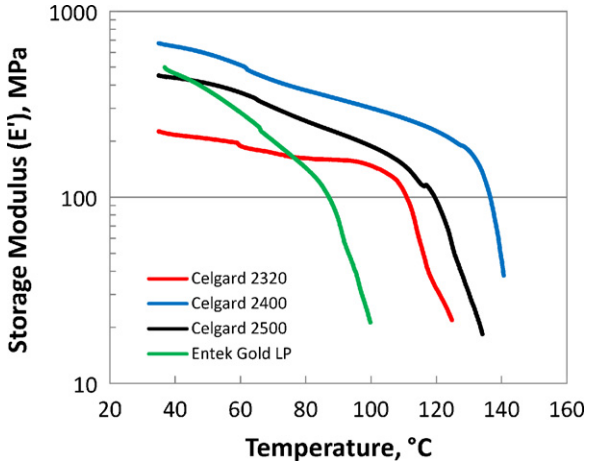

Fig. 6. Dynamic thermomechanical analysis of storage modulus vs. temperature polymer separators loaded in tension in the transverse orientation.

Table 3
Thermomechanical transition temperatures for polymer separators under static loading in the as-received condition and after the electrolyte soak environment.

Condition	Temperatures, °C[a]	Celgard® 2320	Celgard® 2400	Celgard® 2500	Entek® Gold LP
As received	Shrink	113.1	134.5	131.3	107.0
	Equilibrium ($\varepsilon = 0$)	130.6	151.5	154.5	125.3
	Deformation	150.6	164.9	166.6	170.4
	Rupture	164.0	168.5	170.0	178.0
Electrolyte soak	Shrink	115.0	132.7	129.9	95.0
	Equilibrium ($\varepsilon = 0$)	132.5	150.0	156.0	118.1
	Deformation	151.4	165.7	167.6	169.8
	Rupture	165.0	169.1	170.9	178.0

[a] All temperatures accurate to within ±1 °C.

Table 4
Dynamic thermomechanical transition temperatures and mechanical properties of polymer separators: as-received, electrolyte soak, annealing, and 100 cycles. The shrink temperatures under static loading for as-received and electrolyte soaked are also give for reference.

Condition	Property[a]	Celgard® 2320	Celgard® 2400	Celgard® 2500	Entek® Gold LP
As received	E' Transition, °C	108.8	133.5	118.1	86.7
	Temperature @ ε_{max}, °C	112.0	136.0	123.7	85.2
	ε_{max}, %	1.02	1.24	1.25	0.41
	E' @ ε_{max}, MPa	90.9	109.2	65.9	114.3
	Shrink temp, static load, °C	113.1	134.5	131.3	107.0
Electrolyte soak	E' transition, °C	111.1	144.1	130.9	92.1
	Temperature @ ε_{max}, °C	114.1	146.2	131.3	59.4
	ε_{max}, %	1.01	1.38	1.12	.08
	E' @ ε_{max}, MPa	124.7	125.4	133.6	505.7
	Shrink temp, static load, °C	115.0	132.7	129.9	95.0
55 °C anneal	E' transition, °C	104.0	131.9	122.3	95.5
	Temperature @ ε_{max}, °C	106.4	133.4	123.0	95.5
	ε_{max}, %	0.64	1.14	1.11	0.64
	E' @ ε_{max}, MPa	50.1	121.1	76.5	70.7
Cycling	E' transition, °C	91.5	134.2	119.4	85.0
	Temperature @ ε_{max}, °C	94.2	136.4	119.1	65.5
	ε_{max}, %	0.69	1.5	0.96	0.11
	E' @ ε_{max}, MPa	75.5	96.8	17.15	214.9

[a] All temperatures accurate to within ±1 °C.

however only in the midsection of the tensile specimen. The transparent area is the region of high localized strain that occurs during necking. The thicker PP samples, Celgard 2400 and Celgard 2500 along with UHMWPE Entek Gold LP did not undergo this transparent transformation. However, the contact point between the tensile fixture and the sample (indicated by transparent horizontal lines) turned transparent as a result of moderate clamping pressure. Celgard 2500 and Entek Gold LP showed the best dimensional stability under dynamic loading at high temperature.

The dimensional stability of the separators tested under dynamic loading is given in Fig. 8. The percent strain as a function of temperature show clear transition points of maximum strain. Max strain peaks indicate the transition from tensile elongation to pore shrinking. The temperature and strain data for dynamic loading is shown in Table 4 along with the shrink temperatures under static loading for reference. The peak strain temperature for all polymer separators are within a few degrees of the transition temperatures observed in the storage modulus data. Therefore, in addition to a dimensional loss there is also a mechanical stiffness loss associated with the onset of pore structure collapse and shrinking. The peak strain temperatures for Celgard 2320 and Celgard 2400 are close to the transition temperatures observed for the static loading condition. Celgard 2500 and Entek Gold LP undergo a dimension transition (peak strain temperature) under dynamic load before transitions are observed under static loading. Entek Gold LP undergoes only 0.41% strain in the as-received condition and is the most dimensionally stable separator.

3.3.1. *Effects of temperature, electrolyte, cycling on mechanical durability*

The strain-to-failure behavior for separators after the 55 °C anneal is different than in the initial as-received condition. The percent ε_{max} is decreased as a result of the low temperature thermal treatment. However, the temperature at ε_{max} does not follow any particular trend. The Celgard separators experience peak strain just below the transition temperatures observed for the as-received condition. The ε_{max} and temperature at ε_{max} for electrolyte soaked polymer separators Celgard 2320 and Celgard 2500 closely relate to those in the as-received condition. The peak strain and peak strain temperatures are both increased for Celgard 2400 under dynamic testing. The Entek Gold LP separator displays a large negative strain with a peak positive strain of only $\varepsilon_{max} = 0.08$. This is nearly the strain experienced for the cycled Entek Gold LP where $\varepsilon_{max} = 0.11$. The temperature at ε_{max} for Entek Gold

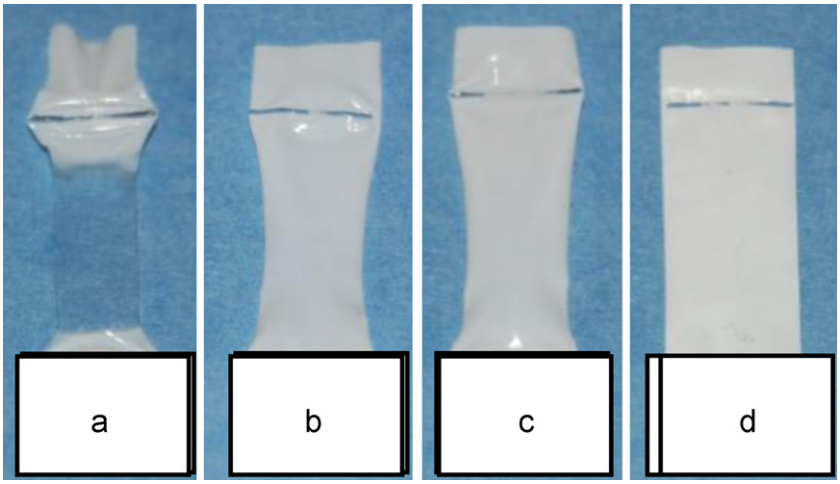

Fig. 7. Dynamic thermomechanical loading of polymer separators: (a) Celgard 2320; (b) Celgard 2400; (c) Celgard 2500 and (d) Entek Gold LP.

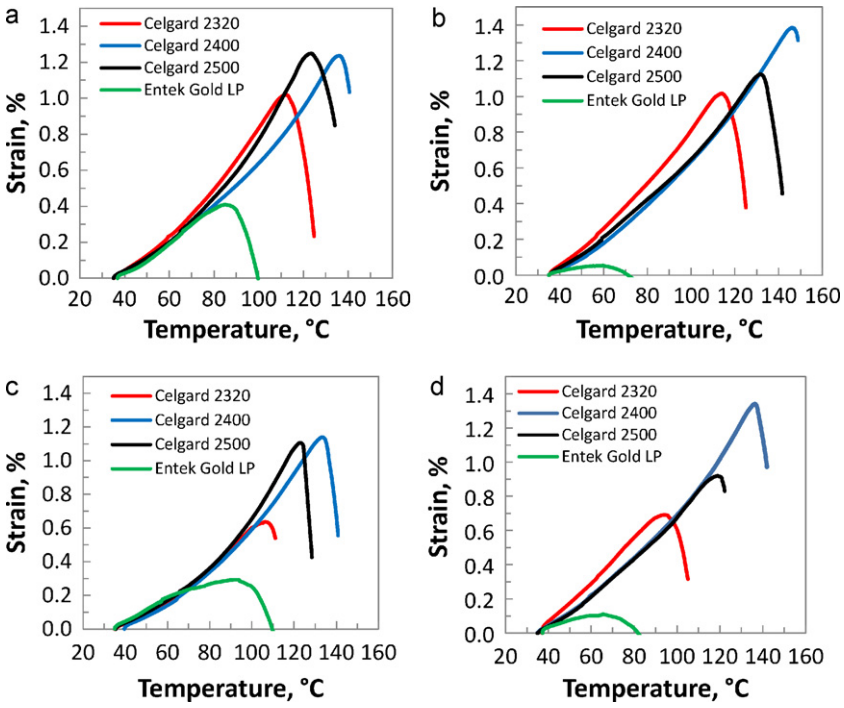

Fig. 8. Strain vs. temperature behavior of dynamically loaded polymer separators illustrating the transition temperature at Max strain: (a) as received; (b) electrolyte soak; (c) 55 °C anneal; and (d) after cycling.

LP decreases under dynamic loading just as observed for static mechanical loading. A significant decrease in the peak strain temperature is likely due to initial swelling of the polymer separator. Above 50 °C the solvent is released removing the artificial elastic strain. The severity of the dynamic loading caused this transition to occur at lower temperature than in the static loading condition.

4. Conclusions

Thermomechanical analysis was performed with a DMA instrument to identify thermal and mechanical transitions for polymer separators under static and dynamic mechanical loading. Clear transitions were observed indentifying changes in deformation mode and the onset of separator "shutdown." The application of static and dynamic mechanical loads causes pore shrinking and thermal shutdown to occur below the polymer melting point. The loading direction was critical to the overall mechanical integrity of the separator. Anisotropic separators (Celgard 2320, 2400 and 2500) were mechanically limited in the transverse direction. This anisotropicity is a result of the manufacturing process used to create the micro-porous membranes. The separator prepared by wet technique (Entek Gold LP) behaved more uniformly, or biaxial, where all mechanical properties were nearly identical within the separator plane. The information provided by the DMA is valuable for predicting the long-term durability of polymer separators in lithium-ion batteries exposed to electrolyte (solvent and salt), thermal fluctuations and electrochemical cycling. Small losses in mechanical performance were observed for separators exposed to the various immersion environments over the 4-week immersion time. Longer immersion times at more severe temperatures would provide valuable information to predict the long-term mechanical and thermal stability of the polymer separators. The most severe mechanical losses for all polymer separators were observed under dynamic mechanical loading while modest losses were observed under static tension.

Acknowledgements

Funding for this work was provided by the Jerome Karle Fellowship at the Naval Research Laboratory. The author acknowledges Celgard LLC and Entek Membranes LLC for donating the sample materials for testing. The author would like to thank Dr. James Thomas of NRL for technical expertise and use of DMA instrument and Dr. Karen Swider-Lyons of NRL for helpful discussions.

References

[1] E.P. Roth, D.H. Doughty, D.L. Pile, J. Power Sources 174 (2007) 579–583.
[2] Y.S. Chung, S.H. Yoo, C.K. Kim, Ind. Eng. Chem. Res. 48 (2009) 4346–4351.
[3] P. Arora, Z.J. Zhang, Chem. Rev. 104 (2004) 4419–4462.
[4] G. Venugopal, J. Moore, J. Howard, S. Pendalwar, J. Power Sources 77 (1999) 34–41.
[5] S. Srinivas, P. Brant, Y. Huang, D.R. Paul, Polym. Eng. Sci. 43 (2003) 831–849.
[6] R.T. Chen, C.K. Saw, M.G. Jamieson, T.R. Aversa, R.W. Callahan, J. Appl. Polym. Sci. 53 (1994) 471–483.
[7] S.-Y. Lee, S.-Y. Park, H.-S. Song, Polymer 47 (2006) 3540–3547.
[8] T. Sarada, L.C. Sawyer, M.I. Ostler, J. Membr. Sci. 15 (1983) 97–113.
[9] D. Djian, F. Alloin, S. Martinet, H. Lignier, J.Y. Sanchez, J. Power Sources 172 (2007) 416–421.
[10] R.S. Baldwin, National Aeronautics and Space Administration, Glenn Research Center, Cleveland, OH, 2009, p.9.
[11] S.S. Zhang, J. Power Sources 164 (2007) 351–364.
[12] Celgard, LLC, Charlotte, NC, 2008.
[13] M.J. Weighall, J. Power Sources 34 (1991) 257–268.
[14] F.G.B. Ooms, E.M. Kelder, J. Schoonman, N. Gerrits, J. Smedinga, G. Calis, J. Power Sources 97–98 (2001) 598–601.
[15] L.H. Sperling, Introduction to Physical Polymer Science, 3rd ed., John Wiley & Sons, New York, 2001.
[16] K.P. Menard, Dynamic Mechanical Analysis: A Practical Introduction, CRC Press, 1999.
[17] K. Cho, D.N. Saheb, J. Choi, H. Yang, Polymer 43 (2002) 1407–1416.
[18] Y.L. Joo, O.H. Han, H.-K. Lee, J.K. Song, Polymer 41 (2000) 1355–1368.
[19] R. Kostecki, L. Norin, X. Song, F. McLarnon, J. Electrochem. Soc. 151 (2004) A522–A526.
[20] Y.M. Pleskachevskii, S.V. Shil'ko, D.A. Chernous, Mech. Compos. Mater. 39 (2003) 129–136.
[21] Celgard 2400 Technical Information Brochure, Celgard, LLC, Charlotte, NC 2008.
[22] Celgard 2500 Technical Information Brochure, Celgard, LLC, Charlotte, NC 2008.
[23] Teklon Certificate of Analysis, ENTEK Membrane LLC, Lebanon, OR 2009.